RSC Advances

PAPER

View Article Online
View Journal | View Issue

Cite this: *RSC Adv.*, 2017, **7**, 25867

A facile one-step fabrication of a novel Cu/MoS_2 nano-assembled structure for enhanced hydrogen evolution reaction performance†

Jiamu Cao,[a] Jing Zhou,[a] Yufeng Zhang*[ab] and Xiaowei Liu[ab]

Received 8th February 2017
Accepted 9th May 2017

DOI: 10.1039/c7ra01605k

rsc.li/rsc-advances

The design and synthesis of non-precious-metal catalysts for the efficient electrochemical transformation of water into molecular hydrogen in acid environments are of paramount importance in reducing energy losses during the water splitting process. Here, unique hybrid nanostructures of Cu/MoS_2 have been prepared by a one-pot microwave-assisted synthesis. The resultant nano-assembled catalyst has excellent hydrogen evolution reaction (HER) electrocatalytic properties, including an overpotential of as low as 120 mV, a Tafel slope of 55 mV dec^{-1}, and a remarkable cycling stability. The observed outstanding catalytic performance can be attributed to Cu nanoparticles (NPs) that improved not only the electrical conductivity of the catalyst but also the catalytic activity by a synergistic effect with the edge exposed, nano-sized MoS_2. These findings confirmed that this earth-abundant material was a useful catalyst for water splitting.

1. Introduction

Hydrogen is a scalable and renewable energy that, once produced, is environmentally and climatically clean over the entire length of its conversion chains, from production to utilization.[1] These advantages are enough to make it a promising alternative energy source to address the existing environmental emission issues from fossil energy.[2] Due to its sustainability, water splitting has become one of the most promising approaches for hydrogen production.[3] During the HER, the advanced electrocatalyst is a key component that reduces the overpotential of electrodes to be low enough that they match the solar photon flux, producing a high current density and consequently increasing the yield of this important electrochemical process.[4] To date, Pt-group metals have been the most effective catalysts in HER.[5,6] However, the high material costs and limited resource of these catalysts hinder the hydrogen economy.[7–9] Alternative low-cost materials for such applications are still in urgent demand.[10,11]

Molybdenum disulfide (MoS_2), a typical member of transition metal sulfides, has a layered structure held together by weak van der Waals forces. It is abundant, geographically ubiquitous, and a potentially cheap graphene analogue material.[12] Recent reports that investigated MoS_2 found it to be a competitive electrocatalyst for HER, and both computational and experimental data suggested that the edge sites of MoS_2 nanoparticles are the active sites, so interest in using MoS_2 as water-splitting electrocatalyst has intensified.[13–15] However, the poor intrinsic conductivity of MoS_2 materials is a matter of concern because it suppresses charge transport.[16,17] Taking this factor into account, we hypothesized that designing MoS_2-based materials with more active edge sites and good conductivity would be an effective way to improve the electrocatalytic HER.

Earth-abundant Cu-based materials have recently attracted more attention, particularly due to their favourable electrical conductivity and low-cost.[18] Meanwhile, according to a volcano plot of the exchange current density as a function of the DFT-calculated Gibbs free energy of adsorbed atomic hydrogen, the value of Cu just lies below those of the noble Pt-group metals.[19] The combination of Cu with MoS_2 appears to be a promising way to increase the conductivity and improve the HER performance. Herein, compared with the Cu/MoS_2-based catalyst reported in previous works,[20,21] we have creatively directly prepared the Cu/MoS_2 nano-assembled structure for high HER activity using a more facile one-step microwave-assisted synthesis.

2. Experimental details

2.1 Preparation of Cu/MoS_2 nano-assembled structure

The Cu/MoS_2 nano-assembled structure (NAS) was prepared by the one-step microwave-assisted method. Sodium molybdate (242 mg), thiourea (286 mg), and $CuCl_2 \cdot 2H_2O$ (2.18 mg) were added to 60 mL of a mixture solution of isopropyl alcohol and ethylene glycol (EG) (v/v = 1 : 4) and sonicated for 30 min. A 1 M NaOH/EG solution was added to the mixture until a pH of 12 was

[a]*MEMS Center, Harbin Institute of Technology, Harbin, China. E-mail: yufeng_zhang@hit.edu.cn*

[b]*Key Laboratory of Micro-systems and Micro-Structures Manufacturing, Ministry of Education, Harbin, China*

† Electronic supplementary information (ESI) available: Experimental details. See DOI: 10.1039/c7ra01605k

reached, and then argon was blown into the mixture for 20 min. The mixture was microwaved for 120 s at a dynamic power of 1700 W by a microwave oven (Panasonic NE-1753) in a draught cupboard and then cooled naturally. Next, 1 M dilute nitric acid was added until a pH of 2 was reached. The product was collected by vacuum filtration and vacuum-dried at 60 °C. For comparison, Cu-modified MoS_2 nanosheets (Cu/MoS_2 NSs) were fabricated by using a similar method to that described above, but with the sodium molybdate and thiourea replaced by 20 mg of MoS_2 NSs. (The detailed synthesis procedure of the MoS_2 NSs and the Cu/MoS_2 NSs material can be found in the ESI section.† The TEM images of the MoS_2 NSs were shown in Fig. S1.†)

2.2 Material characterization

The morphologies of the electrocatalysts were observed by transmission electron microscopy (TEM) using a microscope operated at an accelerating voltage of 300 keV. X-ray diffraction (XRD) profiles of Cu/MoS_2 NAS with high-intensity Cu Kα radiation ($\lambda = 1.5406$ nm) in the range of 10–90°. X-ray photoelectron spectroscopy (XPS) was used to record the elemental composition and the electron binding energy using a K-Alpha instrument.

2.3 Modification of the glassy carbon electrode

4 mg of the synthesized Cu/MoS_2 NAS catalysts and 80 μL of 5 wt% Nafion solution were dispersed in 1 mL of a water/ethanol mixture (3 : 1 v/v) followed by a sonication for 15 min to obtain a homogeneous catalytic slurry. Afterward, a glassy carbon electrode (GCE) with a diameter of 3 mm, which was polished by alumina suspensions, was treated with 5 μL of the catalytic slurry and dried at a temperature of 26 °C (loading 0.285 mg cm^{-2}). In addition, Cu/MoS_2 NSs, MoS_2 NSs, small-sized MoS_2 NSs and Pt/C modified electrodes were prepared by the same method for comparison purposes.

2.4 Electrochemical evaluation

The HER activities of these catalysts were evaluated *via* linear sweep voltammetry (LSV) in 0.5 M H_2SO_4 solution at a scan rate of 5 mV s^{-1} and at a temperature of 26 °C. All electrochemical measurements were conducted using an electrochemical workstation (CHI 660D) and a standard three-electrode setup containing a saturated calomel electrode (SCE) as the reference electrode, a graphite rod as the counter electrode, and the modified GCEs as working electrodes. The AC impedance measured in the frequency range between 10^6 Hz and 0.02 Hz with an AC voltage of 5 mV. Before electrochemical measurement, all polarization curves reported in our work were treated for IR loss and all of the potentials were calibrated to a reversible hydrogen electrode (RHE) by adding a value of (0.241 + 0.059pH) V and the utilized electrolytes were degassed by bubbling Ar gas for 1 h.

3. Results and discussion

The morphologies of Cu/MoS_2 NAS and Cu/MoS_2 NSs were characterized by transmission electron microscopy (TEM). Fig. 1a gives a close-up view of Cu nanoparticles (NPs) uniformly distributed on MoS_2. The mean size of Cu NPs, extracted by directly measuring 138 particles from the TEM, is estimated to be approximately 5.8 nm. Fig. 1b shows an HRTEM image of the Cu/MoS_2 NAS with a lattice spacing of 0.24 nm, corresponding to the (111) plane of Cu.[22] Also visible is the clear lattice fringes of MoS_2. As shown in Fig. 1c and Fig. S2,† TEM was used to observe the morphology of Cu/MoS_2 NSs, in which Cu NPs (with a diameter of 12.5 nm) aggregated on the surface of MoS_2 NSs. HRTEM (Fig. 1d) indicated that having many highly crystalline Cu NPs covering the edges of MoS_2 NSs may lead to the reduction of HER electrocatalytic performance.

Fig. 2a shows the XRD pattern of the Cu/MoS_2 NAS. For the pattern of the sample, the peaks at $2\theta = 14.2°$, 33.0°, 39.7°, and 59.1° are attributed to the (002), (100), (103) and (110) planes of MoS_2.[23] The peaks of Cu at 43.5°, 50.5° and 74.5° in the range of 40–80° can be assigned to the diffraction from the (111), (200), (220) planes of reductive Cu NPs with cubic phase, respectively.[24] XPS spectra were recorded to gain further insights into the chemical nature and bonding state of the Cu/MoS_2 NAS. As shown in Fig. 2b, the high-resolution Mo 3d XPS spectrum contains two strong characteristic peaks at 228.9 eV and 231.9 eV, which can be attributed to the Mo^{4+} oxidation state,[25] while the relatively weak peak detected at 235.7 eV corresponds to the Mo^{6+} oxidation state (the latter feature most likely resulted from the formation of a very small amount of MoO_3 species during catalyst preparation). Hence, the majority of the synthesized Mo species exhibited an oxidation state of +4. Furthermore, the high-resolution S $2p_{1/2}$ and S $2p_{3/2}$ spectra, which were centred at 161.8 eV and 162.9 eV, respectively, revealed the presence of divalent S^{2-} ions (Fig. 2c).[26] After peak deconvolution of Cu $2p_{3/2}$ in Fig. 2d, XPS spectrum peaks centred at 935.4 and 932.7 eV can be assigned as CuO and Cu_2S.[27]

Different polarization curves obtained for the studied catalysts *via* LSV are shown in Fig. 3a. It was found that the Pt/C

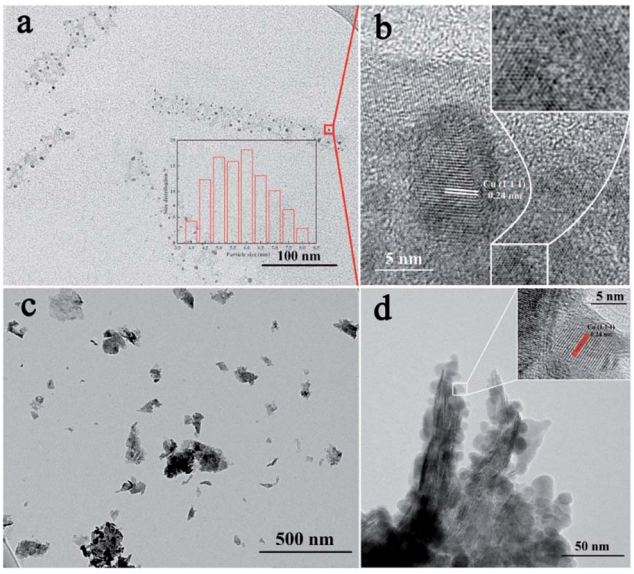

Fig. 1 TEM images of Cu/MoS_2 NAS (a) and Cu/MoS_2 NSs (c). HRTEM images of Cu/MoS_2 NAS (b), and Cu/MoS_2 NSs (d).

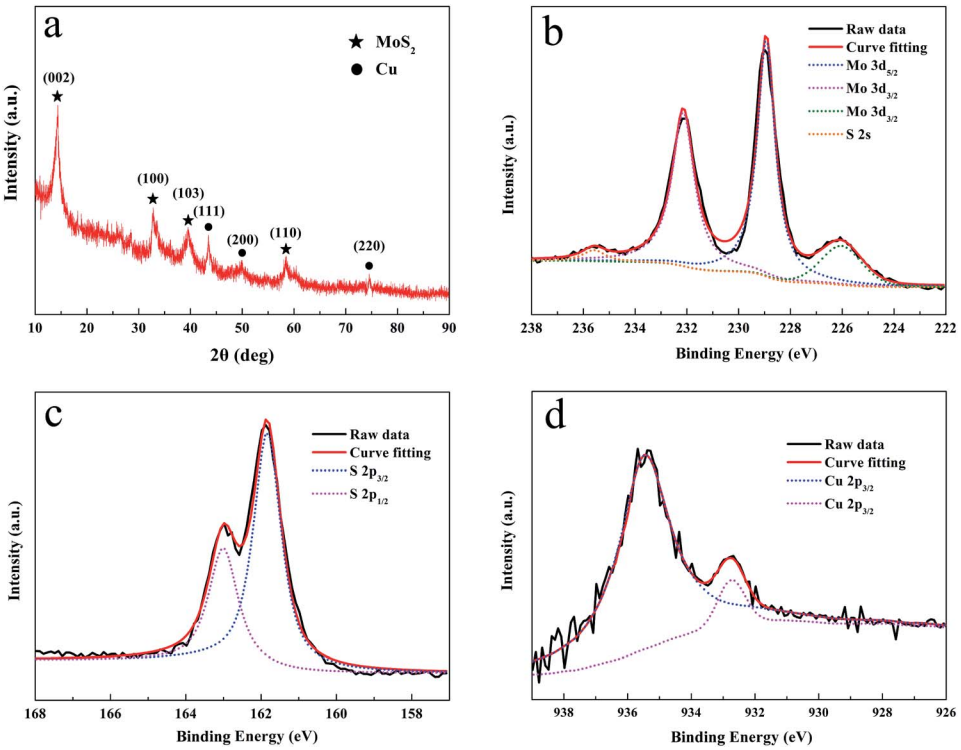

Fig. 2 XRD pattern of Cu/MoS_2 NAS (a). XPS images of Mo 3d (b), S 2p (c), and Cu 2p (d).

catalyst exhibited very strong HER performance with an overpotential close to zero, while the Cu/MoS_2 NAS was characterized by a small overpotential of approximately 120 mV. For comparison, small-sized MoS_2 NSs without $CuCl_2 \cdot 2H_2O$ are fabricated by using a similar method to that described for Cu/MoS_2 NAS synthesized (Fig. S3 and S4†). In a sharp contrast, both the Cu/MoS_2 NSs, pure MoS_2 NSs, and small-sized MoS_2 NSs exhibited poor HER electrocatalytic activity. The linear segments of the corresponding Tafel plots (Fig. 3b) were fit with the Tafel equation $\eta = b \times \lg j + a$, where j is the current density, and b is the Tafel slope. As a result, the Tafel slopes of 92, 83, 66, 55, and 34 mV per decade were obtained for MoS_2 NSs, small-sized MoS_2 NSs, Cu/MoS_2 NSs, Cu/MoS_2 NAS, and Pt/C catalyst, respectively. It is indicated that the improved performance of the catalyst is contributed to the introducing of Cu NPs which is in accordance with previous reports.[20,21] The high HER catalytic activity of the prepared Cu/MoS_2 NAS catalyst can be attributed to the strong electronic coupling between the Cu and MoS_2. To maximize this effect, impedance measurements were performed at an overpotential of $\eta = 120$ mV. As shown in Fig. 3c, the same amount of the Cu/MoS_2 NAS catalyst exhibited an alternating current impedance of approximately 275 Ω, which was much lower than that of the MoS_2 NSs (approximately 1800 Ω) and Cu/MoS_2 NSs (approximately 370 Ω).

To further evaluate the long-term stability of the synthesized Cu/MoS_2 NAS catalyst, cyclic voltammetry (CV) measurements by scanning 2000 cycles from −300 mV to 300 mV (*vs.* RHE) with a scan rate of 100 mV s^{-1} in an acidic environment (0.5 M H_2SO_4) was used. Fig. 3d shows the comparison of polarization curves of the catalyst during the first cycle and 2000th cycle. The almost overlapped curves indicate the negligible loss of the catalytic performance and a remarkable stability of the Cu/MoS_2 NAS catalyst.[28] In addition, the TEM images depicted in the insert of Fig. 3d show that the original morphology of the hybrid catalyst was well preserved after acidic treatment.

Remarkably, Tafel slopes are one of the most significant factors that can discern the HER mechanism. According to the classic theory,[29] Tafel slopes for the typical Volmer, Heyrovsky, and Tafel reactions are around of 120 mV dec^{-1}, 40 mV dec^{-1}, and 30 mV dec^{-1}, respectively (1–3). The following are the now accepted steps by which HER in acidic aqueous media described, where MH_{ads} represents a hydrogen atom chemically adsorbed on an active site of various material (M). In view of the Tafel slope of 55 mV dec^{-1} for the Cu/MoS_2 NAS catalyst in the current work, a combination of the Volmer reaction, involving an electrochemical desorption step that converts protons into absorbed hydrogen atoms on the catalyst surface, and the Heyrovsky reaction, involving the formation of surface scope hydrogen molecules, should dominate the HER on the catalytic process of the Cu/MoS_2 NAS catalyst. In other words, the rate determining step is the electrochemical desorption of H_{ads} and H_3O^+ to form hydrogen, and the HER occurs through a Volmer–Heyrovsky mechanism.

$$H_3O^+ + e^- + C \rightarrow MH_{ads} + H_2O \quad (1)$$

$$H_3O^+ + e^- + MH_{ads} \rightarrow C + H_2 + H_2O \quad (2)$$

$$MH_{ads} + MH_{ads} \rightarrow 2M + H_2 \quad (3)$$

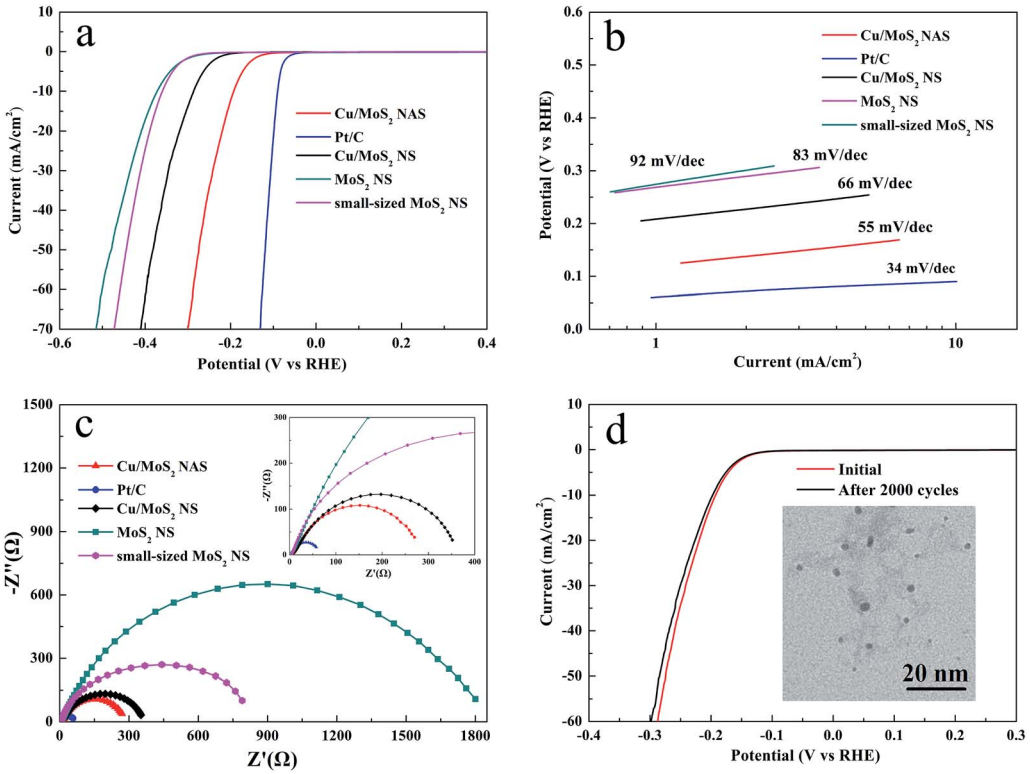

Fig. 3 Polarization curves for catalysts (a) and the corresponding Tafel plots (b). Impedance spectroscopy at an overpotential of 120 mV (c). Durability test for the Cu/MoS_2 NAS (d).

To elucidate the synergistic effect produced by the synthesized Cu/MoS_2 NAS catalyst on the catalytic process in more detail, a simple model (Fig. 4) can be considered. The obtained hybrid contains a large number of active HER catalytic sites due to the abundance of accessible edges resulting from the small size and irregular shape of MoS_2. The use of Cu NPs not only improved the electrical conductivity of the catalyst but also further enhanced the catalytic activity by a synergistic effect with nano-sized MoS_2. Therefore, the produced Cu/MoS_2 NAS catalyst can effectively reduce dissociated H^+ ions and release H_2 molecules on a large number of active sites.

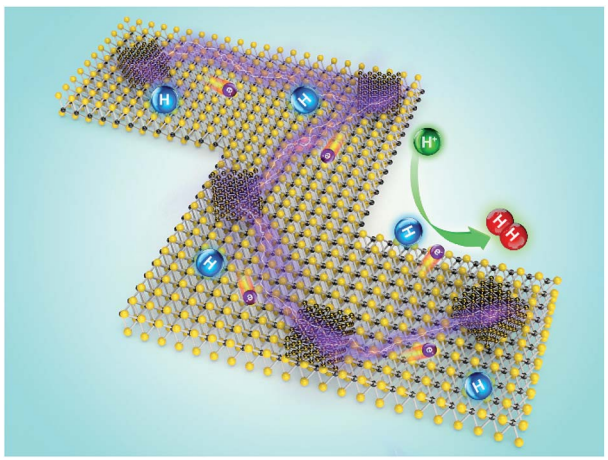

Fig. 4 Schematic illustration of the mechanism governing the electrocatalytic HER on the Cu/MoS_2 NAS.

4. Conclusions

In summary, a facile microwave-assisted method has been used to synthesize a Cu/MoS_2 NAS catalyst for HER. TEM images show that Cu NPs can disperse on MoS_2 uniformly, which improves conductivity. The Cu/MoS_2 NAS exhibits excellent HER catalytic properties and long cycle life, which is attributed to the excellent electrical coupling between the Cu NPs and the nano-sized MoS_2. Therefore, this work describes an inexpensive method for the efficient fabrication of a Cu/MoS_2 NAS catalyst for the HER.

Acknowledgements

The work described in this paper was financially supported by the National Natural Science Foundation of China (No. 61404037 and No. 61376113).

Notes and references

1 H. I. Karunadasa, C. J. Chang and J. R. Long, *Nature*, 2010, **464**, 1329–1333.
2 J. A. Turner, *Science*, 2004, **305**, 972–974.
3 J. S. Luo, J. H. Im, M. T. Mayer, M. Schreier, M. K. Nazeeruddin, N. G. Park, S. D. Tilley, H. J. Fan and M. Grätzel, *Science*, 2014, **345**, 1593–1596.

4 M. G. Walter, E. L. Warren, J. R. McKone, S. W. Boettcher, Q. Mi, E. A. Santori and N. S. Lewis, *Chem. Rev.*, 2010, **110**, 6446–6473.
5 C. Chen, Y. J. Kang, Z. Y. Huo, Z. G. Zhu, W. Y. Huang, H. L. Xin, J. D. Snyder, D. Li, J. A. Herron, M. Mavrikakis, M. Chi, K. L. More, Y. Li, N. M. Markovic, G. A. Somorjai, P. Yang and V. R. Stamenkovic, *Science*, 2014, **343**, 1339–1343.
6 T. Ye, L. B. Lv, M. Xu, B. Zhang, K. X. Wang, J. Su, X. H. Lin and J. S. Chen, *Nano Energy*, 2015, **15**, 335–342.
7 Y. Shi, J. Wang, C. Wang, T. T. Zhai, W. J. Bao, J. J. Xu, X. H. Xia and H. Y. Chen, *J. Am. Chem. Soc.*, 2015, **137**, 7365–7370.
8 F. K. Ma, Y. Z. Wu, Y. L. Shao, Y. Y. Zhong, J. X. Lv and X. P. Hao, *Nano Energy*, 2016, **27**, 466–474.
9 W. X. Zhu, C. Tang, D. N. Liu, J. L. Wang, A. M. Asiric and X. P. Sun, *J. Mater. Chem. A*, 2016, **4**, 7169–7173.
10 Y. J. Tang, Y. Wang, X. L. Wang, S. L. Li, W. Huang, L. Z. Dong, C. H. Liu, Y. F. Li and Y. Q. Lan, *Adv. Energy Mater.*, 2016, **6**, 1600116.
11 Y. C. Zhoua, Y. H. Leng, W. J. Zhou, J. L. Huang, M. W. Zhao, J. Zhan, C. H. Feng, Z. H. Tang, S. W. Chen and H. Liu, *Nano Energy*, 2015, **16**, 357–366.
12 B. W. Jin, X. M. Zhou, L. Huang, M. Lickleder, M. Yang and P. Schmuki, *Angew. Chem., Int. Ed.*, 2016, **55**, 12252–12256.
13 T. F. Jaramillo, K. P. Jørgensen, J. Bonde, J. H. Nielsen, S. Horch and I. Chorkendorff, *Science*, 2007, **317**, 100–102.
14 J. Bonde, P. G. Moses, T. F. Jaramillo, J. K. Nørskovb and I. Chorkendorff, *Faraday Discuss.*, 2008, **140**, 219–231.
15 B. Hinnemann, P. G. Moses, J. Bonde, K. P. Jørgensen, J. H. Nielsen, S. Horch, I. Chorkendorff and J. K. Nørskov, *J. Am. Chem. Soc.*, 2005, **127**, 5308–5309.
16 Z. Y. Zhang, W. Y. Li, M. F. Yuena, T. W. Nga, Y. B. Tang, C. S. Lee, X. F. Chenc and W. J. Zhang, *Nano Energy*, 2015, **18**, 196–204.
17 Q. H. Wang, K. K. Zadeh, A. Kis, J. N. Coleman and M. S. Strano, *Nat. Nanotechnol.*, 2012, **7**, 699–712.
18 M. B. Gawande, A. Goswami, F. X. Felpin, T. Asefa, X. X. Huang, R. Silva, X. X. Zou, R. Zboril and R. S. Varma, *Chem. Rev.*, 2016, **116**, 3722–3811.
19 D. Merki and X. Hu, *Energy Environ. Sci.*, 2011, **4**, 3878–3888.
20 F. Li, J. Li, X. Lin, X. Li, Y. Fang, L. Jiao, X. An, Y. Fu, J. Jin and R. Li, *J. Power Sources*, 2015, **300**, 301–308.
21 F. Li, L. Zhang, J. Li, X. Lin, X. Li, Y. Fang, J. Huang, W. Li, M. Tian, J. Jin and R. Li, *J. Power Sources*, 2015, **292**, 15–22.
22 R. Krishna, D. M. Fernandes, J. Ventura, C. Freire and E. Titus, *Int. J. Hydrogen Energy*, 2016, **41**, 11608–11615.
23 G. Du, Z. Guo, S. Wang, R. Zeng, Z. Chen and H. Liu, *Chem. Commun.*, 2010, **46**, 1106–1108.
24 J. Luo, S. Jiang, H. Zhang, J. Jiang and X. Liu, *Anal. Chim. Acta*, 2012, **709**, 47–53.
25 B. J. Guo, K. Yu, H. L. Li, H. L. Song, Y. Y. Zhang, X. Lei, H. Fu, Y. H. Tan and Z. Q. Zhu, *ACS Appl. Mater. Interfaces*, 2016, **8**, 5517–5525.
26 K. C. Pham, Y. H. Chang, D. S. McPhail, C. Mattevi, A. T. S. Wee and D. H. C. Chua, *ACS Appl. Mater. Interfaces*, 2016, **8**, 5961–5971.
27 M. Sam, M. R. Bayati, M. Mojtahedi and K. Janghorban, *Appl. Surf. Sci.*, 2010, **257**, 1449–1453.
28 H. Deng, C. Zhang, Y. Xie, T. Tumlin, L. Giri, S. P. Karna and J. Lin, *J. Mater. Chem. A*, 2016, **4**, 6824–6830.
29 J. G. N. Thomas, *Trans. Faraday Soc.*, 1961, **57**, 1603–1611.